Intelligent Autonomous Systems IAS-3, Pittsburgh, PA, February 1993, pp. 643-652,

Contact Information from Proprioception*

Manfred Huber and Roderic A. Grupen

Laboratory for Perceptual Robotics
Department of Computer Science
University of Massachusetts
Amherst, Massachusetts 01003

Abstract

This paper presents a method to derive estimates of contact properties for the case of a planar robot interacting with unknown objects by means of proprioceptive information (joint angles and torques). In a first stage, two kinematic observations, based on the instantaneous velocities and the displacement between two consecutive postures, are used to obtain an estimate of the location with an associated uncertainty. This is then fused over time by tracking using a linear observer, resulting in a final position estimate. A second step then uses torque domain evidence and the location estimates to decide the existence of the contact and to compute a corresponding contact force estimate. This approach allows the detection of multiple contact points on different links and provides estimates for the contact location, velocity, surface normal and contact force, using general manipulator motions.

1. Introduction

For an autonomous system it is essential to perceive various properties of the world in order to successfully perform a given task. In the case of manipulation tasks, the necessary information includes different aspects of the contacts between the agent and objects in the environment and is required for such actions as object modeling [1], force control in whole-arm manipulators [2] or incremental grasp configuration in dextrous robot hands [3]. One method to obtain this information is by means of tactile perception.

A first approach to tactile perception employs tactile sensor arrays distributed over the manipulator surface [4, 8], similar to tactile receptors in the skin of animals. This, however, leads to packaging problems for the multitude of wires or electronic parts required to transmit the information. The algorithm presented in this paper takes a different approach, namely by making more effective use of available proprioceptive information (joint angles and torques) to replace or supplement tactile array sensors.

Following this line, [2] and [9] describe methods that employ torques of two joints and complete force information (3 forces and 3 moments), respectively, to derive the contact

*This work was supported in part by NSF IRI-9116297 , CDA-8922572 and IRI-9208920

location. Because of the multitude of dynamic effects, however, these systems are very static in the sense that no movements are allowed during the localization. To overcome the problem of noisy torque information, Kaneko and Tanie [6] use torque information only to detect the existence of a contact and initiate then strategic posture changes to determine the contact based on the intersection of two consecutive postures. All these approaches, however, suffer from the fact that they don't allow for general motions and can only detect one contact on the whole manipulator. The algorithm presented in this paper tries to overcome these limitations for the planar case by employing the current motion of the robot arm and fusing the information of multiple observers based on geometric constraints and torque domain evidence.

In the following, Section 2. presents an overview of the algorithm and the individual observers used. Section 3. then shows results obtained using this approach for a dynamic robot simulator and a finger of the Utah/MIT hand.

2. The Algorithm

The algorithm of this paper uses rigid body constraints and the violations of freespace dynamics to infer the location and force of a contact between a planar robot arm with revolute joints and an unknown stationary object. The used manipulator of the type of Figure 1 provides thereby the necessary information in the form of joint angles Θ_i, joint velocities $\dot{\Theta}_i$ and torques τ_i.

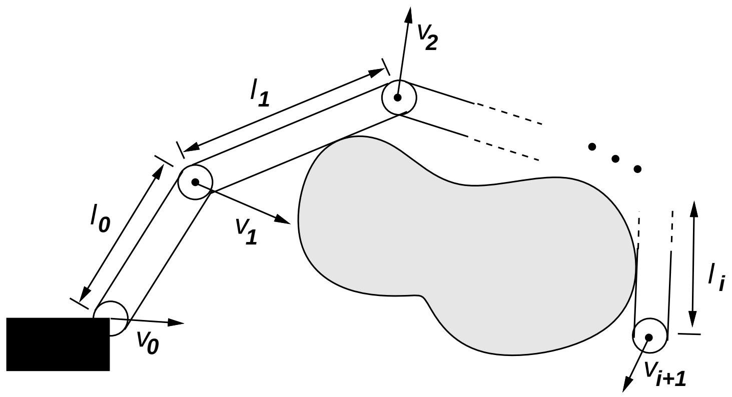

Figure 1: Planar Robot Arm with Object

The algorithm uses geometric constraints to estimate the contact location for each link under the assumption that a contact exists. This contact *localization* is accomplished using two observers based on displacement and velocity, respectively, fused over time by means of a linear estimator. Finally, during contact *detection*, torque domain evidence is used to determine the existence of a contact for each link.

The following sections briefly introduce the main ideas behind the algorithm (for a detailed analysis see [5]). In this description, the properties of the robot will be described by the variables

Θ_i^t	Joint angle
τ_i^t	Joint torque
l_i	Link length
r_i	Half the width of the link
v_i^t	Cartesian velocity of link endpoint

where subscript i indicates the link/joint number and superscript t the time of the observation[1].

2.1 Geometric Properties - Localization

In the localization stage, two observations based on geometric contact constraints are used for each link to obtain an estimate of the contact location which is fused over time in a linear Kalman filter in order to derive the final estimate together with an associated uncertainty. This is done for the link and tip regions separately because of the differences in surface geometry for these two parts. A final step based on additional kinematic constraints tries then to decide if either the link or the tip contact is correct.

2.1.1 Link Contacts

To simplify the analysis, a contact point on the link is represented in internal link coordinates in form of the side s (± 1) of the link and the distance d from the proximal endpoint of the link to the contact location. Figure 2 illustrates these internal coordinates.

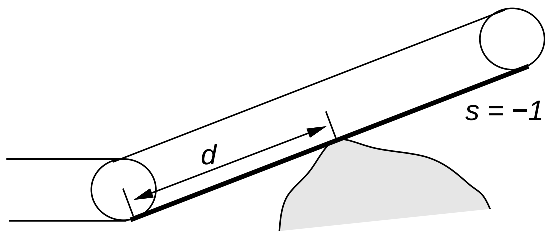

Figure 2: Internal Contact Coordinates

To obtain an estimate of this location, the value of s is determined by torque evidence which is shown in Section 2.2. The parameter d on the other hand is solely based on geometric observations of the moving link. To do this, the projection of the instant center of velocity onto the link surface is used as an initial estimate which is then filtered to cope with uncertainties in the environment, resulting in the final estimate $\hat{d}$ and a corresponding uncertainty measure. The filter used is the linear observer

$$
\begin{aligned}
\hat{d}^t &= \left(\hat{d}^{t-1} + v_c \Delta t\right) + \frac{\hat{\varepsilon}^{t-1} + \varepsilon_{v_c} \Delta t}{\varepsilon_d + \hat{\varepsilon}^{t-1} + \varepsilon_{v_c} \Delta t} \left(d - \left(\hat{d}^{t-1} + v_c \Delta t\right)\right) \\
\hat{\varepsilon}^t &= \frac{\varepsilon_d \left(\hat{\varepsilon}^{t-1} + \varepsilon_{v_c} \Delta t\right)}{\varepsilon_d + \hat{\varepsilon}^{t-1} + \varepsilon_{v_c} \Delta t} \ ,
\end{aligned}
\tag{1}
$$

with,

$$
\begin{aligned}
\hat{d}^t &= \text{Filtered location at time } t \\
d &= \text{Instantaneous center location} \\
v_c &= \text{Contact point velocity on the link} \\
\hat{\varepsilon}^t &= \text{Uncertainty associated with } \hat{d}^t \\
\varepsilon_d &= \text{Uncertainty associated with } d \\
\varepsilon_{v_c} &= \text{Uncertainty associated with } v_c \ .
\end{aligned}
$$

The variables v_c and ε_{v_c} are thereby set to a smoothed version of $\frac{\Delta \hat{d}}{\Delta t}$ and $\frac{\hat{\varepsilon}^t + \hat{\varepsilon}^{t-1}}{\Delta t}$, respectively. The parameter ε_d results from the use of a second geometric observation,

[1]Subscripts and superscripts are avoided wherever possible for simplicity

namely a corrected version of the intersection between two consecutive link postures. Using this second estimate $d^{'}$, a worst case error bound of

$$\varepsilon_d \leq \frac{\hat{\varepsilon}^{t-1}\frac{1}{\varphi}\tan\frac{\varphi}{2} + \left|d^{'} - d\right|}{1 - \frac{1}{\varphi}\tan\frac{\varphi}{2}} \qquad \text{for } \frac{\tan\frac{\varphi}{2}}{\varphi} < 1 \;, \tag{2}$$

where φ is the angle between the two link postures, can be derived under the assumption that the curvature of the object is locally constant. This is used as a bounding error instead of a more sophisticated environmental or sensor model.

2.1.2 Tip Contacts

Tip contacts are represented by the radius r of the spherical tip region and the angle ϕ from the x axis as illustrated in Figure 3.

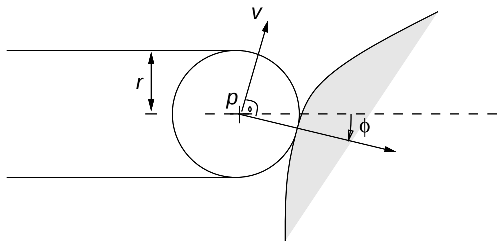

Figure 3: Tip Contact Representation

The estimation process parallels then the one for link contacts where the initial estimate for the filter is given by the fact that the angular contact coordinate ϕ is orthogonal to the Cartesian velocity vector v of the link endpoint. This leads to the linear observer equations

$$\begin{aligned} \hat{\phi}^t &= \left(\hat{\phi}^{t-1} + \omega\Delta t\right) + \tfrac{\hat{\epsilon}^{t-1}+\epsilon_\omega\Delta t}{\epsilon_\phi+\hat{\epsilon}^{t-1}+\epsilon_\omega\Delta t}\left(\phi - \left(\hat{\phi}^{t-1} + \omega\Delta t\right)\right) \\ \hat{\epsilon}^t &= \tfrac{\epsilon_\phi\left(\hat{\epsilon}^{t-1}+\epsilon_\omega\Delta t\right)}{\epsilon_\phi+\hat{\epsilon}^{t-1}+\epsilon_\omega\Delta t} \;, \end{aligned} \tag{3}$$

where,

$\hat{\phi}^t$ = Filtered location at time t
ϕ = Location hypothesis from velocity vector
ω = Angular contact point velocity
$\hat{\epsilon}^t$ = Uncertainty associated with $\hat{\phi}^t$
ϵ_ϕ = Uncertainty associated with ϕ
ϵ_ω = Uncertainty associated with ω .

The values for ω and ϵ_ω are given by $\frac{\Delta\hat{\phi}}{\Delta t}$ and $\frac{\hat{\epsilon}^t+\hat{\epsilon}^{t-1}}{\Delta t}$, respectively. To determine the remaining unknown ϵ_ϕ, a second estimate is used to derive an expression for the worst case error. The location hypothesis in this case is given by choosing the angular contact representation ϕ orthogonal to the displacement vector of the link endpoint in two consecutive posture recordings. Using a corrected version $\phi^{'}$ of this value leads to the error bound

$$\epsilon_\phi \leq \hat{\epsilon}^{t-1} + 2\left|\phi^{'} - \phi\right| \tag{4}$$

for the linear observer of Equation 3.

2.1.3 Link/Tip Decision

The separate treatment of the link and tip regions results in two location estimates for each link. It is therefore necessary to decide which of these two positions is the correct one. This is achieved by means of additional kinematic constraints on the location and movements of the contact points [2]. Measures of the degree of violation of these constraints are used as counterevidence for either one of the two contacts. The decision process for the experiments presented in Section 3. is done by a simple linear combination of three values of this type.

2.2 Dynamic Properties - Detection

All the geometric analysis above was done under the assumption that a contact exists on each link. To verify the existence of such a contact, however, torque domain evidence has to be used as a third observation in order to allow general manipulator motions.

2.2.1 Torque Decomposition

Every contact between a manipulator and an object produces a contact force and therefore a unique set of joint torques which violate the freespace dynamics of the robot. Given a dynamic model of the manipulator [3] and the locations and interaction forces of more distal contacts, it is therefore possible to compute the torques due to contacts on proximal links. This torque value τ for the most distal of these allows to decide the existence and side s for a potential contact by means of

$$s = sign(\tau) \ . \tag{5}$$

The contact force can also be calculated using the torque and the location given by the geometric considerations of Section 2.1.

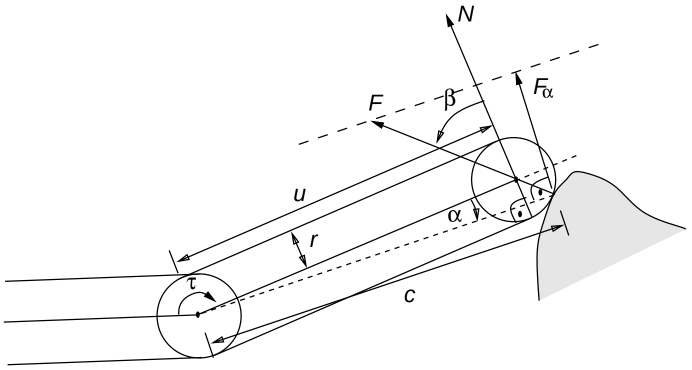

Figure 4: Contact Force Construction

The properties shown in Figure 4 lead to a contact force F in direction of the surface normal of magnitude

$$|F| = \frac{|\tau|}{\sqrt{(u + r\sin\beta)^2 + (r\cos\beta)^2} \cdot \cos(\alpha+\beta)} \ , \tag{6}$$

[2]This can not succeed in general because manipulator motions for both contact types can be identical.

[3]Because of the way torque information is used, only a worst case model is necessary.

where

$$\left.\begin{array}{ll} u & = \hat{d} \\ \beta & = (s+1)\,\frac{\pi}{2} \end{array}\right\} \text{for link contacts}$$
$$\left.\begin{array}{ll} u & = l \\ \beta & = \frac{\pi}{2} + \hat{\phi} - \sum_{j=0}^{i} \Theta_j \end{array}\right\} \text{for tip contacts .}$$

It is therefore possible to compute contact forces for one contact per link, starting from the most distal link.

2.2.2 Uncertainties and Friction

To cope with uncertainties in the dynamic model and the contact locations, the extrema of these values are propagated into intervals of possible torques. Taking a conservative approach, a contact is then verified only when all torque values indicate a violation of the freespace dynamics. Since Coulomb friction can be seen as an uncertainty in the direction of the contact force (represented by the friction cone), it can be incorporated in the same way by changing the angle β in Equation 6 to $\beta \pm \vartheta$ where $\tan\vartheta$ represents the maximum coefficient of friction.

3. Experiments

3.1 Simulations

This section presents results obtained from a dynamic robot simulator, using an elastic object model. Compliant motion of the finger is generated by a PD controller, regulating the finger's position relative to reference angles $\Theta_{ref_i} = \pi/4$ while the finger's coordinate frame is displaced with a constant speed ($0.33 m/s$) in the negative x-direction. To illustrate the performance of the algorithm, both smoothly curved and polygonal objects are presented.

Figures 5-7 show sequences of snapshots of the robot interacting with an object and the data obtained during this movement. The radii of the circles representing the contact estimates denote the associated uncertainty obtained by the Kalman filter of the localization part. The statistics on the right show probability distributions for the absolute distance between the object surface and the hypothesized contact points.

In the case of the circular object presented in Figure 5, all the estimates are up to $0.6mm$ inside the object (recall that this is an elastic object and that the manipulator must push on it to observe it).

The performance degrades slightly for the polygonal object shown in Figure 6.

For this convex polygon 2.1% of the estimates lie more than $2mm$ outside the object. The main reason for this can be seen in the fact that the contact points are not necessarily moving continuously over the arm surface, therefore violating one of the assumptions of the Kalman filter. Setting the absolute error in relation to the error estimate, however, shows that the error exceeds the uncertainty estimate for only 1.1% of the points.

As a third object, Figure 7 shows the results for a concave object.

For similar reasons as in the second example, the results here show 5.6% of the points more than $2mm$ outside the object, still denoting for an acceptable performance and illustrating the applicability of this approach for different kinds of object shapes.

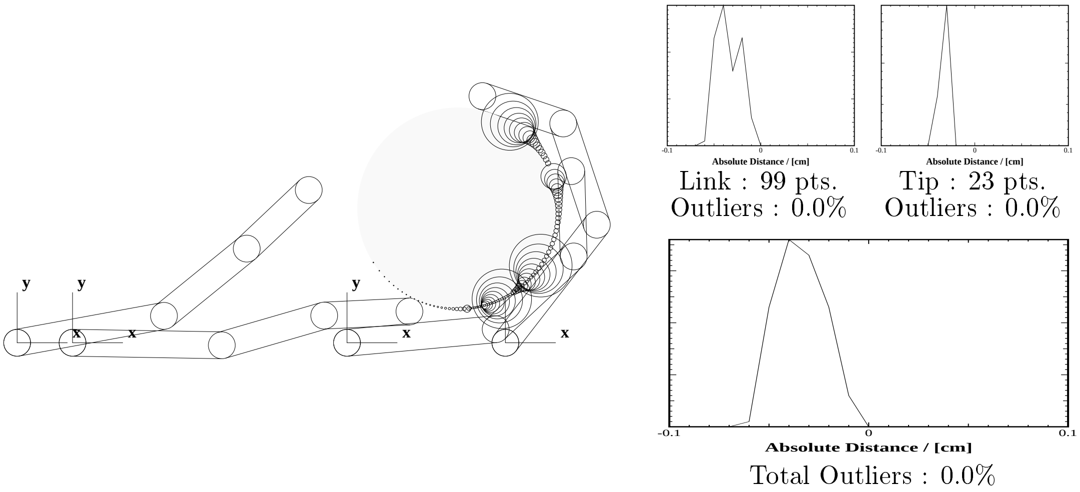

Figure 5: Absolute Distance Error for Spherical Object

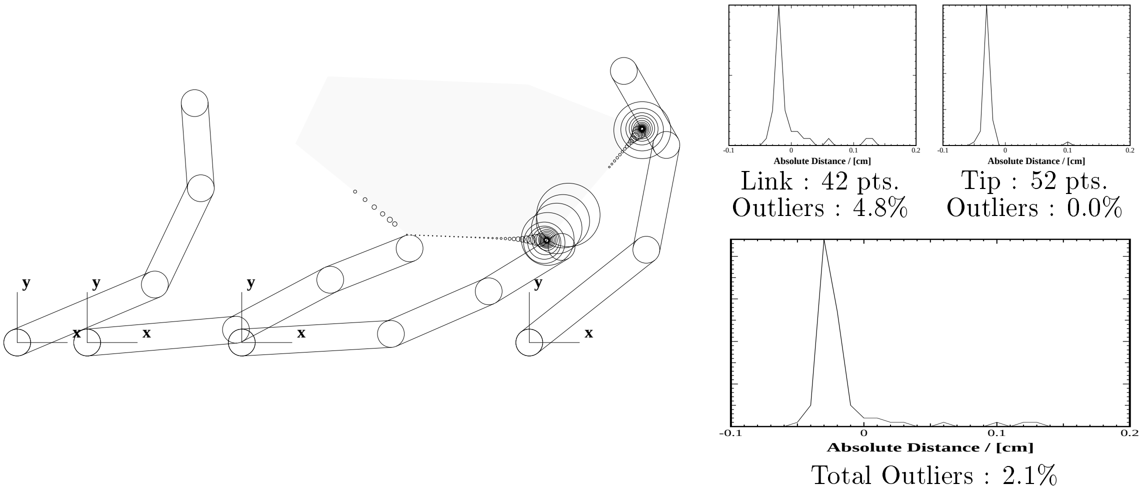

Figure 6: Absolute Distance Error for Polygon

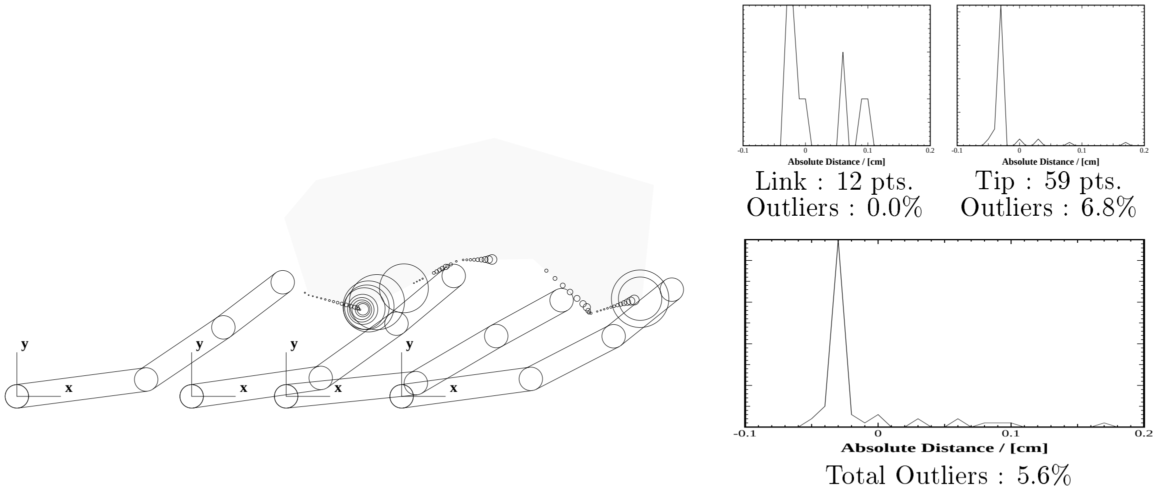

Figure 7: Absolute Distance Error for Polygon

3.2 Robot Experiments

This section shows first results using the index finger of a Utah/MIT dextrous hand mounted on a GE P50 robot, the only change done to the algorithm being the adaptation to the conical link geometry of the manipulator. Torque information for these experiments is calculated from the tendon tensions using a decoupling matrix (see [7]). In this initial stage of robot experiments, constant upper and lower thresholds are used as a worst case dynamic model while straight line movements and compliance are achieved by motions of the GE P50 and a PD controller, regulating the finger's position relative to constant reference angles, respectively. Objects are fixed to a table in order to prevent them from moving.
Figure 8 shows a sequence of snapshots of the finger interacting with a cylindrical object. The black circles in the right picture show the contact estimates, where the radii represent the associated uncertainty.
Similarly, Figure 9 presents results for a rectangular peg, again showing the applicability of the algorithm even for small manipulators with a different geometry.
The data obtained from these initial experiments shows higher uncertainties for the estimates than in the simulations while the location estimates still remain close to the actual contact point. Some of this additional uncertainty can be attributed to additional noise appearing on the sensors of the robot and to friction. A second problem can be seen in the choice of the control gains for the finger. If these are chosen to high, the resulting interaction forces will cause the object to move. The gains for these initial experiments are therefore rather low, thereby decreasing the signal to noise ratio in the torque information. All this suggests room for improvement in future experiments.

4. Conclusions

This paper presented a method to calculate contact information for a planar robot using general motions and proprioceptive information and requires therefore no complex hardware like tactile sensor arrays. The data obtained from simulations and real experiments using a Utah/MIT hand suggests that this method could be used for various tasks to replace or supplement hardware sensors.

Acknowledgments

The authors would like to thank Kamal Souccar for his help with the robot implementation and all the members of the Laboratory for Perceptual Robotics for their support.

REFERENCES

[1] P.K. Allen. Integrating vision and touch for object recognition tasks. *International Journal of Robotics Research*, 7(6):15–33, 1988.

[2] S.J. Gordon and W.T. Townsend. Integration of tactile-force and joint-torque information in a whole-arm manipulator. In *Proceedings of the IEEE International Conference on Robotics and Automation*, pages 464–469, Scottsdale, AZ, May 1989. IEEE.

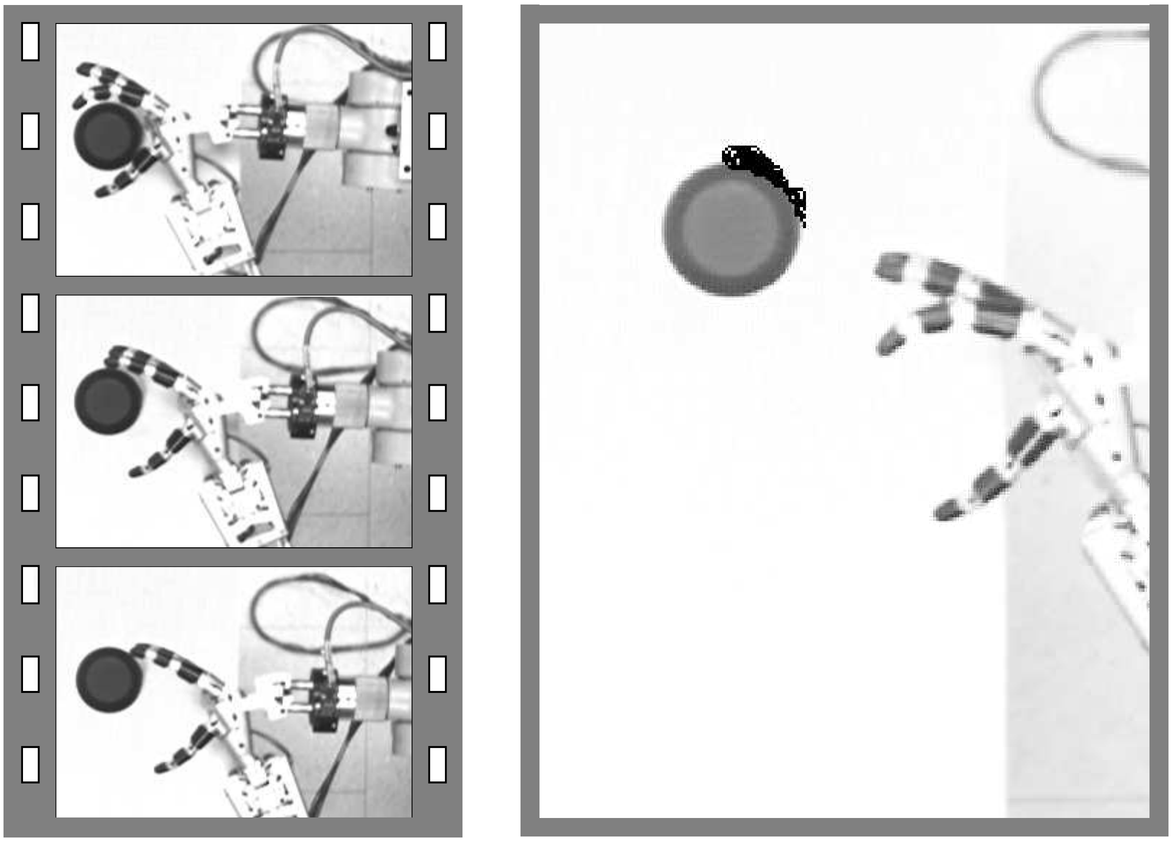

Figure 8: Utah/MIT Hand with Circular Object

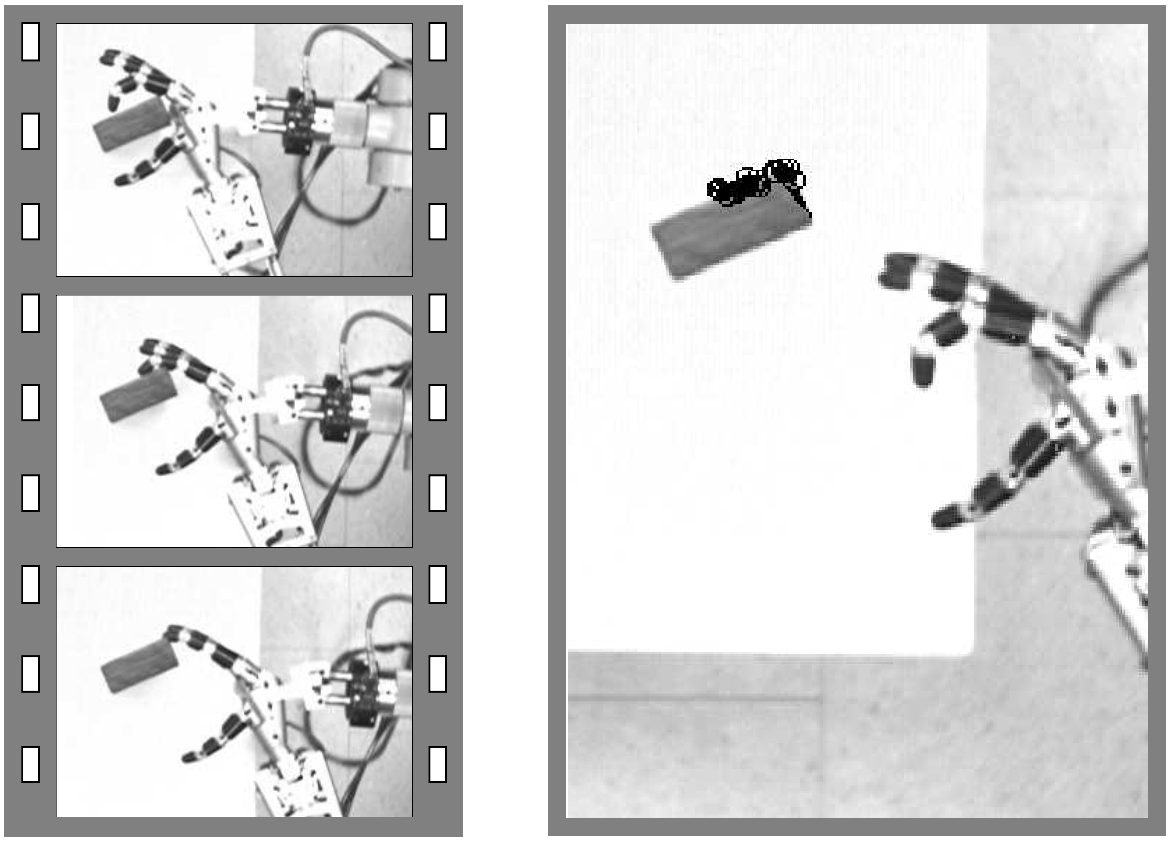

Figure 9: Utah/MIT Hand with Rectangular Object

[3] R.A. Grupen. Planning grasp strategies for multifingered robot hands. In *Proceedings of the IEEE International Conference on Robotics and Automation*, pages 646–651, Sacramento, CA, April 1991. IEEE.

[4] R.A. Grupen, T.C. Henderson, and I.D. McCammon. A survey of general purpose manipulation. *International Journal of Robotics Research*, 8(1):38–62, 1989.

[5] M. Huber and R.A. Grupen. 2-d contact detection and localization using proprioceptive information. Technical Report 92-59, Department of Computer Science, University of Massachusetts, Amherst, August 1992.

[6] M. Kaneko and K. Tanie. Contact point detection for grasping of an unknown object using self-posture changeability (spc). In *Proceedings of the IEEE International Conference on Robotics and Automation*, pages 864–869, Cincinnati, OH, May 1990. IEEE.

[7] S. Narasimhan. Dextrous robotic hands: Kinematics and control. Technical Report AI TR 1056, Massachusetts Institute of Technology, 1988.

[8] H.R. Nicholls and M.H. Lee. A survey of robot tactile sensing technology. *International Journal of Robotics Research*, 8(3):3–30, 1989.

[9] T. Tsujimura and T. Yabuta. A tactile sensing method employing force/torque information through insensitive probes. In *Proceedings of the IEEE International Conference on Robotics and Automation*, pages 1315–1320, Nice, France, May 1992. IEEE.